OPEN ACCESS

University of BRISTOL

Peer reviewed version

Link to published version (if available):
10.1021/acsabm.9b00608

Link to publication record in Explore Bristol Research
PDF-document

University of Bristol - Explore Bristol Research
General rights

The Effect of Matrix Stiffness of Biomimetic Gelatin Nanofibrous Scaffolds on Human Cardiac Pericyte Behaviour

Mincy Raj Naduthottathil, [†] Elisa Avolio,[‡] Michele Carrabba,[‡] Sean Davis,[§] Massimo Caputo,[‡] Paolo Madeddu,[*,‡] and Bo Su[*,∥]

[†]Bristol Centre for Functional Nanomaterials (BCFN), University of Bristol, BS8 1TL, Bristol, U.K

[‡]Bristol Medical School, University of Bristol, Upper Maudlin Street, BS2 8HW, Bristol, U.K

[§]School of Chemistry, University of Bristol, BS8 1TS, Bristol, U.K

[∥]Bristol Dental School, Lower Maudlin Street, BS1 2LY, Bristol, U.K

Corresponding Authors Email:

Bo Su b.su@bristol.ac.uk

Paolo Madeddu mdprm@bristol.ac.uk

ABSTRACT

Congenital heart disease (CHD) is the most common and deadly congenital anomaly, accounting for up to 7.5% of all infant deaths. Survival in children born with CHD has improved dramatically over the past several decades, this positive trend being counterbalanced by the fact that more patients develop heart failure. Seminal data indicate an alteration of the extracellular matrix occurs with time in these hearts due to diffuse and abundant interstitial fibrosis. This results in an escalation in stiffness of the local myocardial microenvironment. However, the influence of matrix stiffness in regulating the function of resident human stromal cells has not been reported. The objective of this study was to determine the impact of scaffold stiffness on the antigenic and functional profile of cardiac pericytes (CPs) isolated from patients with CHD. To this end, we have first manufactured gelatin nanofibrous scaffolds with varying degree of stiffness using an *in situ*-cross-linking electrospinning technique in pure water solvent system. We assessed the Young's Modulus and performed a comprehensive physicochemical characterisation of the scaffolds employing Scanning Electron Microscopy and Fourier- Transform Infrared Spectroscopy. We next evaluated the changes induced by different scaffold stiffness on CP morphology, antigenic profile, viability, proliferation, angiocrine activity, and induced differentiation. Results indicate that soft matrixes with a fiber diameter of ~400nm, increase CP proliferation, secretion of Angiopoietin 2, and F-actin stress fiber formation, without affecting antigenic profile, viability, or differentiation. These data indicate for the first time that human CPs can be functionally influenced by slight changes in matrix stiffness. The study elucidates the importance of mechanical/morphological cues in modulating the behaviour of stromal cells isolated from patients with CHD.

KEYWORDS: *in situ*-cross-linking electrospinning, matrix stiffness, cardiac pericytes, stem cells, cardiac differentiation

1
2
3
4
5
6
7
8
9
10
11
12
13
14
15
16
17
18
19
20
21
22
23
24
25
26
27
28
29
30
31
32
33
34
35
36
37
38
39
40
41
42
43
44
45
46
47
48
49
50
51
52
53
54
55
56
57
58
59
60

3

1. INTRODUCTION

The native extracellular matrix (ECM) can be regarded as a dynamic and hierarchically organised nanomaterial that not only provides mechanical support for embedded cells, but also interacts with the cells and regulates cellular functions such as adhesion, migration, proliferation, and differentiation.[1] A typical ECM is composed of structural protein nanofibers such as collagen, with dimensions ranging from tens to hundreds of nanometers in a three-dimensional form.[1-3] ECM biomimetics, recently developed for tissue engineering therapeutics, expectedly play a similar role in supporting cell viability and growth *in vitro* as native ECM does *in vivo.* [4, 5]

Studies of cell culture systems are principally focused on chemical cues, i.e. cell-binding proteins and peptides, or topographical cues, i.e. nanofibrous form.[6-9] However, increasing evidence suggests mechanical stiffness pivotally modulates the behaviour and fate of cardiac stromal cells, particularly self-renewal and differentiation. It is known that native ECM consisting of collagen or fibrin nanofibers has a much higher local stiffness (elastic modulus of ~MPa at the individual-fibre level) than the bulk ECM (elastic modulus of ~kPa). Therefore, the mechanical stiffness of ECM is not just dependent on its material properties at the individual fibre level but also on its 3D structure. [4, 5, 10-12]

Changes in stiffness occur in the hearts and arterial vessels of patients with congenital heart disease (CHD), currently acknowledged as the most common congenital anomaly responsible for 7.5% of all infant deaths and for an increased heart failure morbidity and mortality.[13] A previous study examining the effects of matrix stiffness on the behaviour of ovine and murine adult cardiac side population cells documented that rigid substrates caused a reduction in cardiomyogenic differentiation, accelerated cell ageing and stimulated the upregulation of extracellular matrix and adhesion proteins gene expression.[14] Nonetheless, to the best of our knowledge, no study has assessed the effect of matrix stiffness on the behaviour

4

of stromal cells from the heart of patients with congenital cardiac defects. Investigating this matter could not only improve the current understanding of cell behaviour during maladaptive heart remodelling but also help to refine the biocompatibility of matrices for tissue engineering correction of cardiac defects.

Cardiac pericytes (CPs) are NG2 and PDGFRb expressing stromal cells that typically locate around capillaries and in close vicinity of coronary arterioles. We have previously reported the antigenic profile, expansion/differentiation capacity, paracrine activity, and pro-angiogenic potential of CPs from neonatal and adult human hearts.[15] In addition, we succeeded in immunosorting and expanding CPs from small biopsies of neonatal human hearts and demonstrated their engrafting capacity in clinically certified prosthetic grafts.[15] There are also preclinical reports showing that pericytes can be effectively used for the repair of the infarcted heart, ischaemic skeletal muscles, and possibly CHD,[16-20] and that 3D hydrogel environment can rejuvenate aged pericytes for skeletal muscle tissue engineering.[21] It is, therefore, crucial to understand how these cells behave in response to mechanical cues in their native environment as well as in artificially modified substrates.

Electrospinning is the most common method used for the fabrication of nanofibers utilizing both natural and synthetic polymers. However, the electrospinnability of gelatin is poor compared to synthetic polymers with defined molecular weight and distribution, such as Polycaprolactone (PCL), Polylactic acid (PLA) and Polylactic-co-glycolic acid (PLGA) as electrospinnability is strongly dependent on polymer chain confirmations and entanglements. Gelatin is polyelectrolytic in nature and possesses a 3-D macromolecular cross-linked network because of the strong hydrogen bonds formed at room temperature, which in turn reduces the mobility of polymer chains.[22] Hence, for the successful electrospinning of gelatin, high-polarity solvents such as 2,2,2,-trifluoroethanol (TFE) and hexafluoroisopropanol (HFIP) are commonly used, which are cytotoxic and expensive.[22,23] This work exploits an alternative

5

biocompatible and cheap water solvent system to obtain gelatin nanofibers using an *in situ*-cross-linking electrospinning method. Despite other conventional cross-linking methods, which often rely on the diffusive reactions of externally added crosslinking agent, *in situ*-cross-linking electrospinning technique with a double-barrel syringe benefits homogeneous mixing of the polymer solution with the crosslinking agent, and hence the formation of uniformly cross-linked gelatin nanofibrous scaffolds. Additionally, this technique will also allow the easy tuning of the requisite amount of cross-linking agent and reduces the unwanted deposition of the cross-linking agent on the surface of the material.

Therefore, in the present study, *in situ*-cross-linked electrospun gelatin nanofibrous scaffolds with different crosslinking densities, prepared in a cheap and biocompatible water system were used as an *in vitro* platform to investigate the effect of matrix stiffness on CP antigenic profile, morphology, viability, proliferation, angiocrine activity and capacity to differentiate into vascular smooth muscle cells (VSMCs).

6

2. MATERIALS AND METHODS

2.1.   Materials

Gelatin from porcine skin (Type A) having a gel strength of 300 was purchased from Sigma Life Sciences UK, glutaraldehyde was obtained from Fischer Biotech UK, double-barrel syringe (10:1) from Sulzer Chemtech UK Ltd, 1-Ethyl-3-(3-dimethylaminopropyl) carbodiimide (EDC) and N-Hydroxysuccinimide (NHS) from Life Technologies Ltd, UK and Sigma Aldrich supplied ninhydrin and glycine.

The materials used for the cell studies were Endothelial Cell Growth Medium 2 (ECGM2, Promocell) supplemented with 2% fetal bovine serum (FBS), Trypsin-EDTA (Life Technologies, UK), 4% Paraformaldehyde (PFA), 0.1% Triton, 40,6-diamidino-2-phenylindole (DAPI) (Sigma-Aldrich) and viability assay kit for live and dead cells (Biotium, UK). All the primary antibodies (Vimentin (1:400), NG2 (1:100) and OCT4 (1:400)) and secondary antibodies (1:200 Alexa 647 Goat anti-Rb and 1:200 Alexa 647 Goat anti-ms) for immunocytochemistry assays were obtained from Abcam. The proliferation assay kits (Click-iT® EdU imaging kits) were procured from Invitrogen and the markers for differentiation assay Calponin (1:100) and α-Smooth Muscle Actin (α-SMA) (1:100) were bought from Abcam and DAKO, UK respectively. The 8mm accupunch was purchased from Schuco International (London) Limited.

2.2.   Fabrication of *in situ*-cross-linked gelatin nanofibrous scaffolds

The gelatin nanofibers with different cross-linking densities were fabricated by using an *in situ*-cross-linking electrospinning technique and a double barrel syringe. The electrospinning set up consisted of a high voltage supply, spinneret and a grounded collector. A hot plate and an ultrasound nebuliser were used to control the environment temperature (40°C) and humidity (>50%). The whole set up was placed in a closed incubator for maintaining the temperature and humidity throughout the process of fabrication.[23]

7

The gelatin solution (15% in water) was taken in a double-barrel syringe (10:1barrel

ratio) with attachable mixing heads (3mm internal diameter and 6cm length) mounted on the

spinneret. Initially, electrospinning was carried out with four different cross-linking densities

of 1-ethyl-3-(3-dimethylaminopropyl) carbodiimide (EDC) and N-hydroxysuccinimide (NHS)

(denoted as 2X, 5X, 8X and 10X, X= 14mM of EDC and 5.5mM of NHS) while maintaining

the concentration of gelatin (15%) and distance between the needle and collector (10 cm)

constant. The gelatin aqueous solution was loaded in the larger barrel, and the smaller barrel

was filled with EDC/NHS crosslinking solution. Both solutions were fed at a fixed rate so that

they could reach the needle at the same time and mix together inside the needle before being

injected to the collector. The homogeneous mixing was achieved with the help of mixing heads

attached to the syringe, and high voltage energy was applied to the solution. A Taylor cone was

obtained when the surface tension of the polymer solution overcame the applied voltage, and

the polymer jet was ejected from the needle. Thus, randomly oriented, internally cross-linked,

gelatin nanofibers were deposited on the grounded collector, which was kept at a fixed distance

(10 cm) from the needle tip. The schematic representation of the electrospinning setup is shown
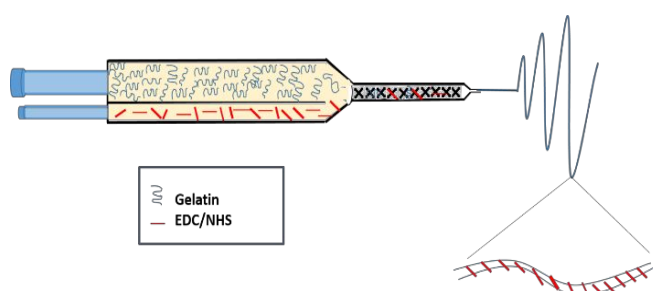
in **Figure 1**.

Figure 1. Schematic representation of double-barrel syringe for producing *in situ* cross-linked gelatin nanofibers during electrospinning. Various cross-linking densities of 1-ethyl-3-(3-dimethylaminopropyl) carbodiimide (EDC) and N-hydroxysuccinimide (NHS) were tested in the study.

Uncross-linked gelatin nanofibers were also fabricated by using the same electrospinning set

up while maintaining the same conditions of temperature and humidity, but the gelatin solution

8

was taken in a 10ml syringe fitted with a needle (21G). These scaffolds were used as the control for further physicochemical characterisation experiments.

Since the scaffolds must be stable for at least three weeks in the cell culture medium for performing the proliferation and differentiation assays, the fabricated *in situ* cross-linked gelatin nanofibrous scaffolds were further cross-linked externally with glutaraldehyde (Glu) vapour (5%) at room temperature by placing the scaffolds in a desiccator. The Glu solution (5ml) was poured at the bottom of the desiccator and kept for 24 hrs to cross-link. After cross-linking, the samples were exposed in a fume hood for 2 hrs and heat treated at 100ºC for 1 hr to remove the residuals of Glu and to partially enhance the cross-linking.[24]

2.3.   Characterisation of gelatin solution and *in situ* cross-linked gelatin nanofibers

2.3.1. Rheology

The rheological characterisation of gelatin solution with different cross-linking densities was performed by using a Bohlin Gemini Rheometer (Malvern Instruments Ltd.).   Viscosity measurements were performed with a cone-plate configuration of geometry CP/40:4° cone angle and 40 mm in diameter. A shear rate of $0.1\text{-}10\text{s}^{-1}$ was applied on a controlled rate to measure the viscosity.

2.3.2. Scanning electron microscopy analysis (SEM)

The structural morphology of fabricated *in situ* cross-linked gelatin nanofibers was analysed using SEM (JEOL IT300). The nanofibers spun on an aluminium foil were cut into small pieces and were fixed on aluminium stubs (12mm) with sticky carbon tapes for observation. All the samples were sputter coated with the silver of thickness 15nm using sputter coater (SC7620, Quorum Technologies, East Grinstead, UK), before performing the SEM analysis. The fiber diameters of the fabricated scaffolds were quantified by using Image J. For this, 20 measurements were taken from each scaffolds and the average fiber diameter was obtained from the histograms (Figure S1).

9

2.3.3. Dissolvability test

The cross-linked gelatin nanofibrous scaffolds were cut into small pieces (2cm x 2cm) and placed in Phosphate Buffer Solution (PBS) for testing the solubility. The samples were taken out at different time intervals (14th and 21st day), air dried, and SEM images were taken to investigate the stability of *in situ* cross-linked gelatin nanofibrous scaffolds.[24] The average fiber diameters of the scaffolds after three weeks immersed in PBS was also calculated by using Image J.

2.3.4. FTIR analysis and Ninhydrin assay

For the FTIR analysis, 2mg of all the samples (uncross-linked gelatin, Glu alone cross-linked gelatin and Glu/EDC/NHS cross-linked gelatin nanofibers) were weighed, and the spectrum analysis was measured in the frequency range of 500 to 4000 cm^{-1} .

For the ninhydrin assay analysis, the gelatin nanofibrous scaffolds with different cross-linking densities of EDC/NHS (2X, 5X, 8X), Glu/EDC/NHS cross-linked scaffolds, and uncross-linked gelatin nanofibrous scaffolds were cut into small pieces (~ 10 mg). All samples were placed in 2 ml of 0.3 M ninhydrin solution and heated at 95°C for 5 min. Then, the absorbance was read at 570 nm using UV-Visible Spectrophotometer (U-1900: Hitachi, Tokyo, Japan) and the degree of cross-linking was calculated by the formula,

$$\text{Cross - linking index (\%)} = (C_b - C_a) / C_b \times 100$$

where C_a - concentration of free amino groups after cross-linking

C_b - concentration of free amino groups before cross-linking

Glycine at various known concentrations was used as standard.[25] All the samples were triplicated for the experiment.

2.3.5. Mechanical characterisation of nanofibrous scaffolds

10

All Glu/EDC/NHS cross-linked, and uncross-linked gelatin scaffolds were mechanically tested using an Instron testing machine. The samples were cut into rectangular pieces of dimensions 10 ± 5 mm in length, 5 ± 3 mm in width and 100 ± 50 μm in thickness, respectively. All samples were triplicated, and measurements were taken using Vernier callipers. Both ends of the samples were attached to a custom-made gripping system which was connected to the mechanical testing device. A strain rate of 1mm/min was applied to the scaffolds until failure, and the stress-strain curves were derived from the force-displacement data. The elastic modulus/stiffness of the fibers was evaluated from the slope of the first linear portion of the stress-strain curve.[26] The mechanical testing of the scaffolds under wet conditions was performed by immersing the samples in a vessel containing water at 37ºC.

2.4.   *In vitro* experiments on human cells

2.4.1. Ethics

Studies complied with the principles stated in the Declaration of Helsinki. The protocol for collection of cardiac leftovers from patients undergoing corrective surgery of congenital heart disease was approved by the North Somerset and South Bristol Research Ethics Committee (REC reference 15/LO/1064). Paediatric patients' custodians gave written informed consent for inclusion in the study. The source and clinical characteristics of the tissue donors are presented in **Table 1**.

Table 1.   Clinical characteristics and pathology of tissue donors used in the study.

Cell Line	Patients Age	Source	Pathology
1	17 months	Right Ventricle	Tetralogy of Fallot (TOF)
2	Three years	Right Atrium	Atrioventricular Canal Septal Defect
3	Three years	Right Ventricle	Atrioventricular Canal Septal Defect
4	Three years	Right Atrium	Mitral Valve Defect

The CPs were isolated, as described by Avolio et al.[15] Briefly, the surgical leftovers of atrium or ventricle specimens from children having congenital heart defects were taken and washed

with PBS. All the specimens were 3 to 5 mm in length and <100 mg in weight. After PBS wash, they were manually minced, and the tissue suspension was incubated for 30 min with 0.45 WU/ml/g Liberase 2 (Roche Technologies, UK). The minced cell suspension was passed through 70, 40, and 30 μm cell strainers subsequently to obtain a single cell suspension. Endothelial cells were separated using anti-CD31 (Miltenyi Biotech) conjugated beads, following the manufacturer's instructions. From the remaining cells, CD34^{+} cells were separated by anti-CD34 beads (Miltenyi Biotech). The obtained cells were cultured in the presence of ECGM2 medium supplemented with 2% fetal bovine serum (FBS). The confluent cells were passaged to new culture dishes, and frozen stocks were generated for the experiments.

All scaffolds were cut into round pieces of 8mm diameter using accu-punch and sterilised before cell seeding. They were immobilised in 48 well plates (CELLSTAR®) using cell crowns (Sigma Aldrich), and sterilisation was attained by soaking the scaffolds in ethanol (70%) for 20 minutes. After PBS wash, the scaffolds were placed under UV light for 30 min. The scaffolds were then immersed in ECGM-2 media containing 2% FBS overnight to remove the residuals of unreacted Glu. Next day, each scaffold was seeded with 20,000 cells.[15] The cells seeded on plastic were used as the control. Four cell lines were used in this work, and all the scaffold samples were duplicated.

2.4.2. Viability Assay

The viability of CPs on the scaffolds was examined by the live/dead assay. It was performed by using the Biotium viability/cytotoxicity assay kit.[15] The viability checks were carried out on the 7th day after seeding the cells. The scaffolds were then stained as per the manufacturer's protocol, and live cell imaging was carried out using a fluorescence microscope (Zeiss).[15] The quantification of viable cells was also performed, and the cell density was calculated using Image J software.

12

2.4.3. Immunocytochemistry (ICC) staining

The ICC staining on CPs was achieved as per the protocol reported by Avolio et al.[15] In short, after two days of incubation in the ECGM2 media, the CPs on the scaffolds were fixed, permeabilised and staining was performed according to the manufacturer's protocol. Briefly, the CPs seeded scaffolds were incubated with primary antibodies (Vimentin, neural/glial antigen 2 (NG2) and octamer-binding transcription factor 4 (OCT4)) for 16 hours at 4°C. Next, the secondary antibody (goat anti-rabbit Alexa Fluor 647) was incubated for 1 hr at 20°C in the dark, followed by the counterstaining of nuclei with 40,6-diamidino-2-phenylindole (DAPI). The scaffolds were then mounted using Fluoromount-G (Sigma-Aldrich), and imaging was accomplished. The quantification of positive cells was established by using Image J software.

2.4.4. Cell adhesion and proliferation studies

SEM was used to observe the morphologies of CPs on scaffolds after seven days of incubation. The scaffolds were fixed and dehydrated through a series of graded ethanol solutions, and air dried.[25] After that, they were silver coated in the vacuum with a thickness of 15nm and were examined by SEM. Backscattered electron detector was used for SEM analysis.

The ability of CPs to proliferate on the scaffolds were evaluated by EdU (5-ethynyl-2′-deoxyuridine) incorporation assay.[26] The EdU detection was performed according to the manufacturer's instructions. Imaging was also carried out by fluorescent microscopy after DNA staining. Image J software was used to find out the percentage of proliferating cells on each scaffold.

2.4.5. Analysis of cell secretome by ELISA

The secretion of angiopoietin-1 (ANG-1), angiopoietin-2 (ANG-2) and Vascular Endothelial Growth Factor (VEGF-A) by CPs was evaluated using ELISA (R&D Systems, UK) of the cultured media collected after 48 hrs of incubation. [15] The data were normalised for the number of cells at the end of the collection time.

2.4.6. Differentiation assay

CPs were exposed to inductive media to promote the differentiation into VSMCs.[15] Initially, the CPs on the scaffolds were cultured in the ECGM2 media. After 48 hours, ECGM2 medium was substituted with ECGM2 medium (basal medium (60% DMEM low glucose + 40% MCDB201) added with 2 ng/ml human Transforming growth factor beta 1 (TGF-β1, Pepro-Tech).[27] The CPs cultured on scaffolds maintained in the ECGM2 media were used as a control. The CPs phenotype was checked at two different time points (7th day and 14th day) after the differentiation was induced. The staining was performed as same as for ICC and the primary antibodies Smooth Muscle (SM)-Calponin and Smooth Muscle alpha-Actin (α-SMA) were used. To quantitatively assess the stress fibers formed by CPs on the scaffolds, the mean intensity of the stained images was measured using Image J. For this, all stained images were converted into grey scale images and were background corrected for standardisation. The mean stress fiber intensity per cell was calculated by selecting different regions in the image and dividing the obtained intensity by the number of nuclei counted.

2.4.7. Statistical analysis

Each experiment was completed in triplicate. GraphPad Prism was used to perform the statistical analysis. The statistical significance was determined by the one-way ANOVA test, and a P-value of < 0.05 was considered as statistically significant. Data are expressed as the mean $\pm$ standard error of the mean (SE).

14

3. RESULTS

3.1. *In situ* cross-linking electrospinning of gelatin nanofibers

In situ cross-linked gelatin nanofibers were produced by optimising the injection flow rate of the polymer solution from the needle to the collector and the applied voltage, while keeping constant the distance between the needle and collector and the polymer concentration. The optimised electrospinning conditions for different concentrations of cross-linking agents EDC/NHS (range from 2 times of 14 mM EDC and 5.5 mM NHS to 8 times of 14 mM EDC and 5.5 mM NHS, denoted as 2X, 5X and 8X) is shown in **Table 2**. Concentrations above this range were not spinnable because of the high viscosity of the solution resulting in the solution getting clogged inside the needle before being emitted to the collector. The viscosity of gelatin polymer solutions with different concentrations of EDC/NHS at a lower shear rate, equivalent to the shear force applied by the syringe (0.11 s^{-1}) is also shown in **Table 2.**

Table 2. **Optimised electrospinning parameters for producing *in situ* cross-linked gelatin nanofibers.** The concentration of cross-linking agents 1-ethyl-3-(3-dimethylaminopropyl) carbodiimide (EDC) and N-hydroxysuccinimide (NHS) was increased from 2 times to 5 and 8 times of 14 mM EDC and 5.5 mM NHS (2X, 5X, and 8X). The cross-linking density of 0X represents the uncross-linked gelatin.

Cross-linking density (mM)	Concentration of gelatin (wt/vol)	Flow rate (ml/min)	Distance (cm)	Voltage (kV)	Viscosity at shear rate 0.11 s^{-1} (Pa.s)
0X	15%	0.003	10	20	0.02
2X	15%	0.025	10	18	47.55
5X	15%	0.010	10	22	64.35
8X	15%	0.007	10	22	129.6

As a control, the pure gelatin nanofibers without cross-linking agents were electrospun in the same *in situ* electrospinning setup, but with a 21G needle. This optimisation protocol was followed by a series of analytical assessments of the produced scaffolds.

3.2. Morphological characterisation of gelatin nanofibers

The fabricated *in situ* cross-linked gelatin nanofibrous scaffolds were then characterised by SEM. The SEM imaging showed that the obtained structures were beads-free and composed of randomly arranged nonwoven fibers (**Figure 2**). They formed a continuous 3D network with interconnected pores similar to the ECM. Control gelatin nanofibers without cross-linking agent were found to have an average diameter of 190±30 nm (**Figure 2 A**). Gelatin nanofibers cross-linked with lower concentrations of EDC/NHS showed a webbed morphology with an average diameter of 398±6 nm and 253±5 nm, respectively (**Figure 2 B&C**). The highest concentration resulted in a uniform structure where fiber junctions were not fused, and fibers had an average diameter of 127±10 nm (**Figure 2 D**). The bar graph in **Figure 2 E** illustrates the reduction in fiber diameter with increasing concentrations of the cross-linking agent probably due to the higher crosslinking degree.

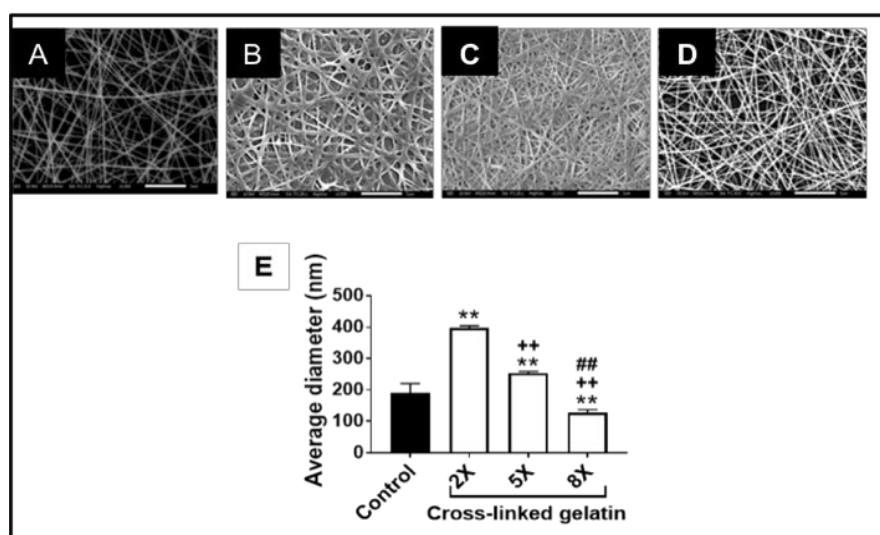**Figure 2. SEM imaging showing the morphology of *in situ* cross-linked gelatin nanofibers: (A-D)** SEM images of uncross-linked gelatin nanofibers (**A**), 2X (**B**), 5X (**C**) and 8X EDC/NHS cross-linked gelatin nanofibers **(D)** . (**E**) Bar graph showing the average fiber diameter with different cross-linking concentrations. Values are mean and SE, N=3 repeats.

16

ANOVA, P<0.01; Tukey's multiple comparisons test adjusted P values: **P<0.01 vs. control, [++]P<0.01 vs. 2X, [##]P<0.01 vs 5X.

3.3. Dissolvability of the scaffolds

Cross-linking agents like EDC/NHS, are reportedly less efficient in maintaining structural stability over 3 weeks. This could preclude the use of scaffolds for tissue/cell engineering applications in the wet condition.[28] Therefore, we tested the dissolvability property of our EDC/NHS scaffolds and verified if this can be improved by the addition of Glutaraldehyde (Glu), which can create stronger aldimine linkages. SEM imaging of as-spun *in situ* cross-linked gelatin nanofibers confirmed the porous and nonwoven fibrous structures of the fabricated scaffolds with different matrix stiffness (**Figure 3 A-C**). After two weeks of immersion in aqueous solution (PBS), the 2X cross-linked gelatin nanofibers were fully dissolved, and the material disappeared, thus demonstrating the instability of this preparation (**Figure 3 D**). Moreover, both 5X and 8X cross-linked gelatin nanofibers changed their morphology to a film, which may be not optimal for the study of how mechanical properties of a given material would affect cell behaviour (**Figure 3 E&F**). Importantly, when the external cross-linking process was accomplished with Glu vapour, the scaffolds retained their structure with a fibrous morphology being observed even after three weeks in PBS (**Figure 3 G-I**). The diameter of the 2X, 5X and 8X Glu/EDC/NHS cross-linked gelatin nanofibers after 3 weeks immersion in aqueous solution were found to be 338±5 nm, 240±3nm and 110±45nm respectively (**Figure 3 J**). Therefore, this fabrication process was further assessed for physicochemical characterization of the scaffolds and studies of tissue engineering with human cells.
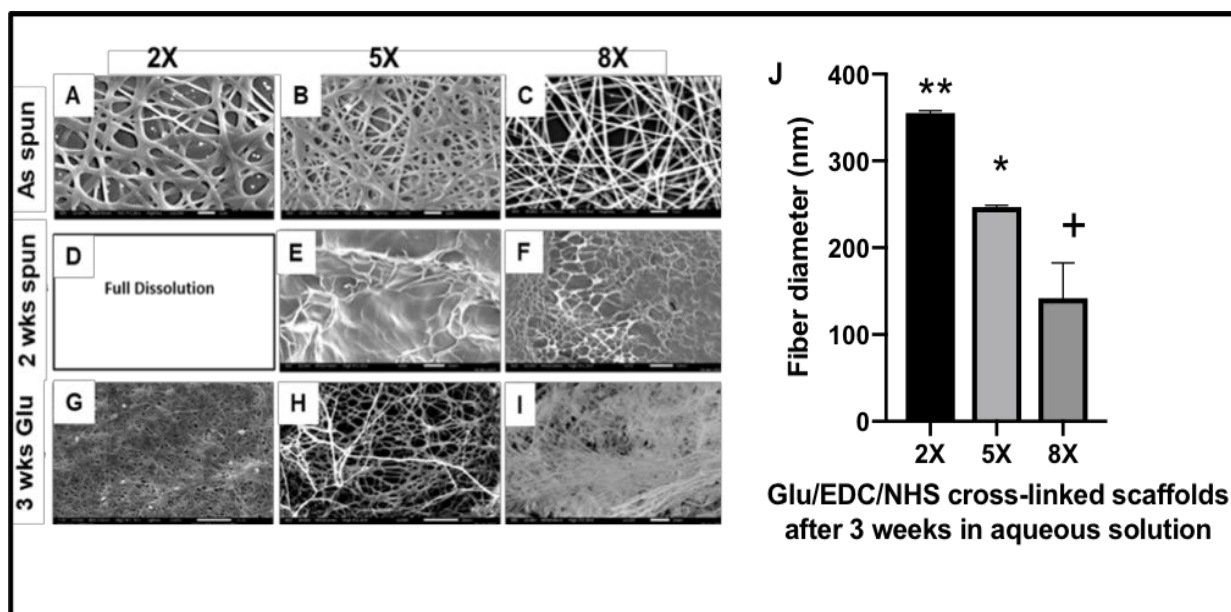
Figure 3. Dissolvability of electrospun gelatin: (**A-C**) As-spun SEM images of 2X, 5X and 8X EDC/NHS cross-linked gelatin nanofibers. (**D-F**) Representative SEM images of 2X, 5X and 8X EDC/NHS cross-linked gelatin nanofibers after two weeks of immersion in PBS. (**G-I**) Retention of fibrous morphology of Glu vapour cross-linked 2X, 5X and 8X EDC/NHS cross-linked gelatin nanofibers after 3 weeks of immersion in PBS. (**J**) Bar graph showing the average fiber diameter of Glu vapour treated 2X, 5X and 8X EDC/NHS cross-linked gelatin nanofibers after 3 weeks of immersion in PBS. Values are mean and SE, N=3 repeats. ANOVA, $P<0.01$; Tukey's multiple comparisons test adjusted P values: *$P<0.05$ vs. 2X, +$P<0.05$ vs. 5X, **$P<0.01$ vs 8X.

3.4. Analysis of structure and cross-linking degree of fabricated scaffolds

Results of the FT-IR spectra of uncross-linked gelatin nanofibers, Glu cross-linked gelatin and Glu/EDC/NHS cross-linked gelatin nanofibers are shown in **Figure 4 A**. The black trace in the Figure shows that the characteristic peaks of gelatin were obtained at 1650 cm^{-1}, which denotes the amide I peak (C=O stretching vibrations), at 1540 cm^{-1}, which corresponds to the amide II peak (N-H bending and C-H stretching vibrations), and at 1240 cm^{-1}, which signifies amide III peak (C-N stretching + N-H in phase bending). Similarly, the characteristic absorption peak for aldimine linkage was observed at 1690 cm^{-1} in the Glu crosslinked gelatin nanofibers (red trace). The peak intensities were much lower for the nanofibers cross-linked with both Glu and EDC/NHS as compared with the Glu alone (blue trace), with the decrease in peak intensity being further enhanced by increasing the concentration of EDC/NHS (pink and green traces).

This phenomenon can be attributed to the EDC/NHS and Glu capability to reduce the amino groups of gelatin. The structure of gelatin was further disturbed when higher concentrations of EDC/NHS (5X and 8X) were used by eliminating Amide III peaks (1240 cm^{-1}), (pink and green traces).

The efficiency of the cross-linking process with the combination of Glu and lowest concentration of EDC/NHS (2X) was estimated using the ninhydrin assay (**Figure 4 B&C**). The ninhydrin reacts with the free amino groups in lysine residues of gelatin nanofibers upon heating thus resulting in the formation of a blue colour. As shown in **Figure 4B**), the intensity of the blue colour faded with increasing concentrations of the EDC/NHS and became yellow in samples cross-linked with Glu\EDC\NHS. Quantification of the data indicates that Glu/EDC/NHS had superior cross-linking activity as compared with the other conditions (**Figure 4C**).
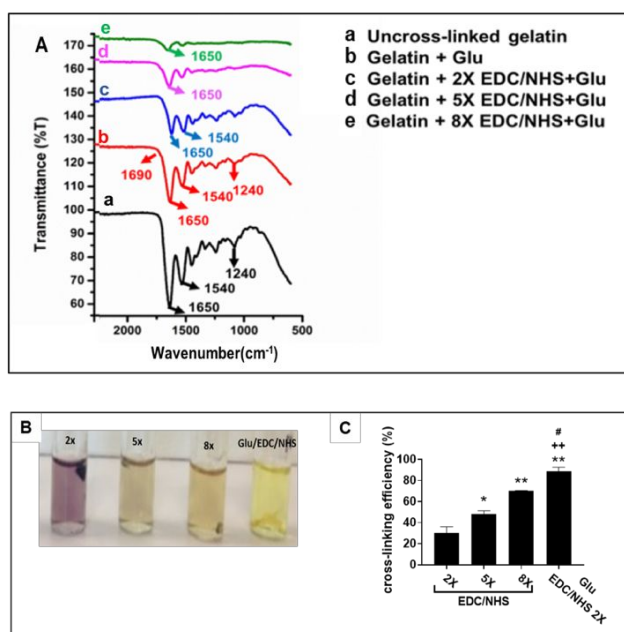
Figure 4. Structure and cross-linking degree of fabricated scaffolds. (A) FT-IR spectra of uncross-linked gelatin (a), Glu cross-linked gelatin (b), and increasing concentrations of Glu\EDC\NHS cross-linked gelatin nanofibers (c, d, and e, respectively). (**B**) Representative image of the colourimetric assay performed on EDC/NHS and Glu/EDC/NHS cross-linked gelatin nanofibers and (**C**) Bar graph illustrating the cross-linking of gelatin nanofibers. Values are mean and SE, N=3 repeats. ANOVA, $P<0.01$; Tukey's multiple comparisons test adjusted P values: *$P<0.05$ and **$P<0.01$ vs. 2X EDC/NHS, [++]$P<0.01$ vs. 5X EDC/NHS, [##]$P<0.01$ vs 8X EDC/NHS.

19

3.5. Mechanical testing of fabricated scaffolds

Finally, the mechanical properties of the scaffolds were measured by calculating Young's modulus (YM) in both dry and wet conditions. In this test, a combination of Glu and increasing concentrations of EDC/NHS was studied. In the dry state, the scaffolds showed progressively higher YM (4 MPa, 10 MPa and 15 MPa) as the concentration of EDC/NHS increased (**Figure 5 A**). This is likely the consequence of the new bonds formed between the functional groups of the polymer, causing the formation of denser and more compact structures. In the wet state, the presence of water contributed to the acquisition of viscoelastic properties and reduction in the YM, which also became remarkably different among scaffolds (**Figure 5 B**). The Glu and 8X EDC/NHS cross-linked scaffolds exhibited an average YM of 0.9±0.3 MPa, which was higher than the other crosslinked scaffolds, showing values <0.3 MPa, or uncross-linked gelatin, whose YM was <0.1 MPa was in agreement with a previous report.[29]
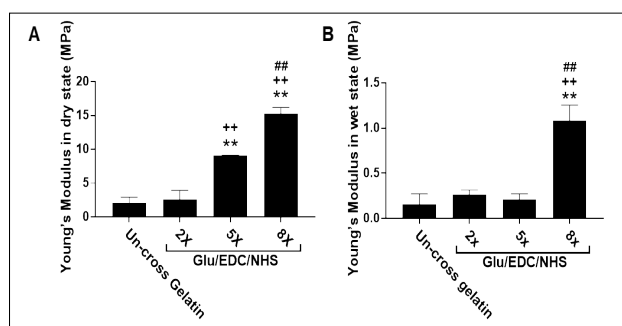
Figure 5. Young's modulus of fabricated scaffolds. (A&B) YM of scaffolds in the dry (**A**) and wet state (**B**). Values are mean and SE, N=3 repeats. ANOVA, P<0.01; Tukey's multiple comparisons test adjusted P values: **P<0.01 vs. un-cross gelatin, ++P<0.01 vs. 2X EDC/NHS, ##P<0.01 vs 5X EDC/NHS.

3.6. Effect of matrix stiffness on CP viability and antigenic expression

Having achieved the fabrication and characterisation of *in situ* cross-linked gelatin nanofibrous scaffolds with varying matrix stiffness, we investigated the scaffold's impact on basic

biofunctional properties of CPs. Cells were obtained from corrective surgery of congenital heart disease.

The live/dead assay was performed to determine whether stiffness can affect the CPs' viability. After 7 days of incubation in the ECGM2 media, the CPs-seeded scaffolds were stained with Calcein AM and EthD III to image the viable and dead cells. The positive controls for live cells (Calcein AM) and dead cells (EthD III) are shown as supporting information (Figure S2). Representative images from fluorescent microscopy indicate CPs were viable in all the preparations (**Figure 6 A-C**) and the quantitative analysis confirmed this observation. None of the scaffolds exhibited dead cells which shows the cytocompatibility of the scaffolds irrespective of their stiffness. The assessment of cell density indicated that the 2X scaffolds (4 MPa) had the highest value (240 ± 40 cells/mm^2) followed by 5X (10 MPa) scaffolds (170 ± 40 cells/mm^2) and 8X (15 MPa) scaffolds (110 ± 10 cells/mm^2) (**Figure 6 D**).

Using immunocytochemistry, we next assessed if variation in stiffness could affect the expression of typical antigenic markers. The CPs seeded on scaffolds were incubated for two days in the ECGM2 media and then permeabilised/fixed for staining with primary antibodies followed by secondary antibody staining. The antigenic phenotype of CPs seeded on glass slides was used as a positive control. As shown in **Figure 6 E-G**, control CPs express Vimentin at the level of the cytoskeleton, NG2 in the plasma membrane, and OCT4 in nuclei, as described previously. [15] This phenotype was conserved when changing the stiffness of the cell substrate (**Figure 6 H-T**). There was however, a change in the CP morphology on 8X scaffolds (15MPa), where cells lost their spindle-shaped aspect and appeared more elongated (**Figure 6 O-Q**).
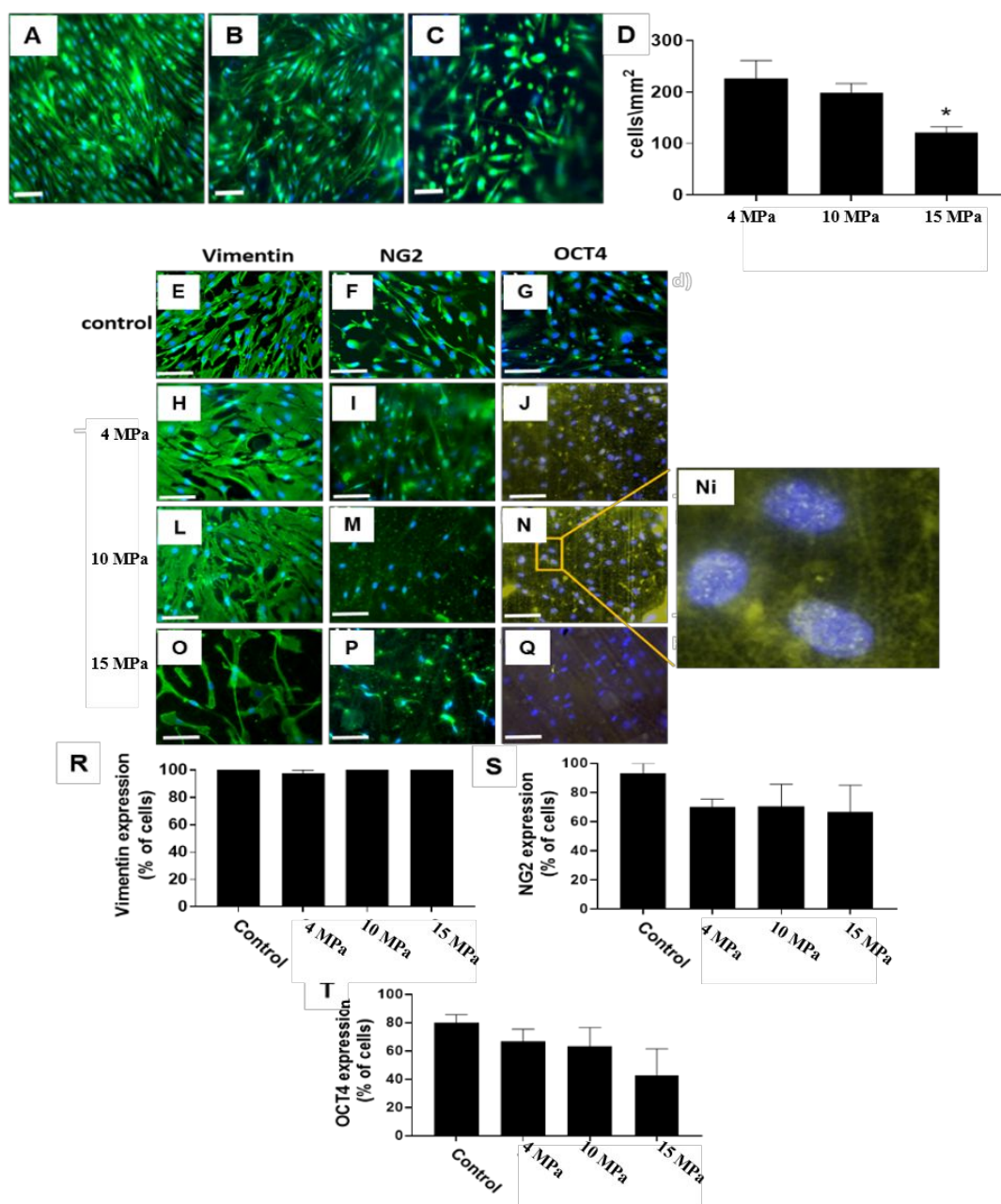
21

Figure 6. Effect of matrix stiffness on cell viability, expression of typical markers, and morphology. (**A-C***)* Live cells are indicated in representative fluorescence images by the cytoplasmic green fluorescence of Calcein, and the blue fluorescence of DAPI representing the nuclei. Scale bar: 50μm. Images are captured after 7 days of culture on 2X (**A**), 5X (**B**), or 8X scaffolds (**C**). (**D**) Bar graph representing the calculated cell density on each scaffold. Values are mean and SE, N=4 cell lines at passage 5 of culture. ANOVA, P<0.05; Tukey's multiple comparisons test adjusted P values: *P<0.05 vs 4 MPa. (**E-Q**) Immunofluorescence characterisation of CPs**.** Fluorescent microscopic images of CPs expressing Vimentin, NG2 and OCT4 on glass slides (**E-G**). Staining for the same markers in CPs seeded on 2X (4 MPa), 5X (10 MPa), and 8X (15 MPa) scaffolds (**H-Q**). An enlarged view of the marked section (**N**) is also shown in (**Ni**), with the fine granules in the nuclei signifying the positive expression of OCT4 in CPs on 5X (10 MPa) scaffolds. Green fluorescence represents the cytoskeleton and blue represents DAPI stained nuclei. Scale bar: 50μm. (**R-T**) Bar graphs showing the results

of the quantification of CPs expressing Vimentin (**R**), NG2 (**S**) and OCT4 (**T**) respectively. Values are expressed as means and SE. N=3 CP lines at passage 5. ANOVA, P=N.S.

To further investigate the morphological changes induced by variation in matrix stiffness, CPs were incubated on scaffolds for seven days and then fixed, dried and sputter coated for SEM analysis. On plastic, CPs exhibited a combination of round and spindle-shaped morphology (**Figure 7**). When seeded on scaffolds, CPs were widespread to generate a 3D cellular network. They conserved the typical spindle-shape with intact cell margins in both 2X (4 MPa) and 5X (10 MPa) scaffolds, while CPs seeded on 8X (15 MPa) scaffolds became elongated and merged into the nanofiber structure (**Figure 7**).
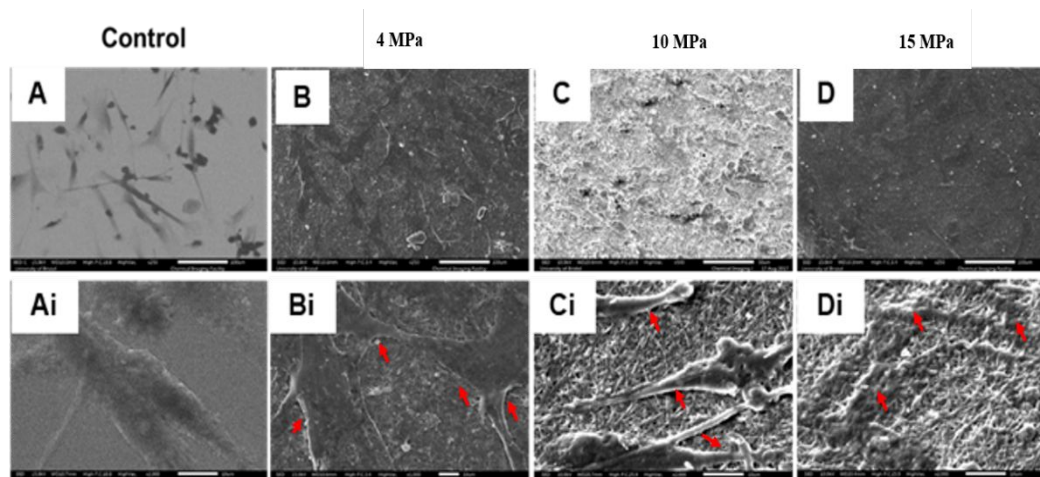

Figure 7. SEM imaging of CPs on the scaffolds of different stiffness. Representative images showing the changes in morphology according to the stiffness of the substrate. Lower panels show magnifications. (**A**) CPs on plastic, (**B-D**) CPs on 2X (4 MPa), 5X (10 MPa) and 8X (15 MPa) Glu/EDC/NHS scaffolds. (**Ai-Di**) represents the corresponding magnified images of the upper panel. The arrow marks in Bi and Ci represents the well-defined cellular margins whereas the arrow marks in the figure Di shows the merged cells.

3.7. Effect of matrix stiffness on CP proliferation and angiocrine function

We next examined the proliferation of CPs on 2X, 5X and 8X scaffolds using the EdU incorporation assay, which is an indicator of active DNA synthesis. In line with the data of cell density illustrated above, the 2X (4 MPa) scaffolds showed a higher number of proliferating CPs as compared to 5X (10 MPa) and 8X (15 MPa) scaffolds (**Figure 8 A-E**). This data demonstrates that CPs prefer to proliferate on a softer substrate. Our previous study indicates

CPs secrete typical angiocrine factors, such as ANG-1, ANG-2 and VEGF-A. [15] The effect of matrix stiffness of the CP angiocrine secretome was assessed by performing ELISA assays on conditioned media collected after 48 hrs from cell seeding. The absolute concentration in media was normalized for the number of the cells to avoid the influence of cell density on results. As shown in **Figure 8 F-H**, CPs seeded on scaffold secreted more abundant quantities of angiocrine factors compared with controls, this difference reaching statistical difference for VEGF and ANG-2 secretion by CPs on 2X (4 MPa) scaffolds.

Finally, we assessed the differentiation capability of CPs into VSMCs on scaffolds with varying matrix stiffness. CPs were seeded on plastic (control) or scaffolds with increasing concentrations of Glu/EDC/NHS and cultured either in the maintenance ECGM2 media (Figure S3) or in differentiation media enriched with TGF-β1 for 7 or 14 days. Only the latter showed the expression of α-SMA and SM-Calponin at both time points, with no difference being noted among the different stiffnesses (**Figure 8 I&J**). Moreover, the actin filaments were found to be widespread, which led to an elongated and extensive distribution of stress fibers on the scaffolds compared to the control. Interestingly, the quantification of stress fiber intensity per cell denoted a significant increase in CPs cultured on 2X (4 MPa) scaffolds as compared with controls and other scaffolds after seven days of incubation in the inductive media (**Figure 8K**). However, on the 14th day, all the scaffolds exhibited the same intensity of stress fibers as that of control (**Figure 8L**). Hence, results suggest that stiffness of the substrate can affect the cytoskeleton organisation of CPs, with softer scaffolds inducing more pronounced effects.
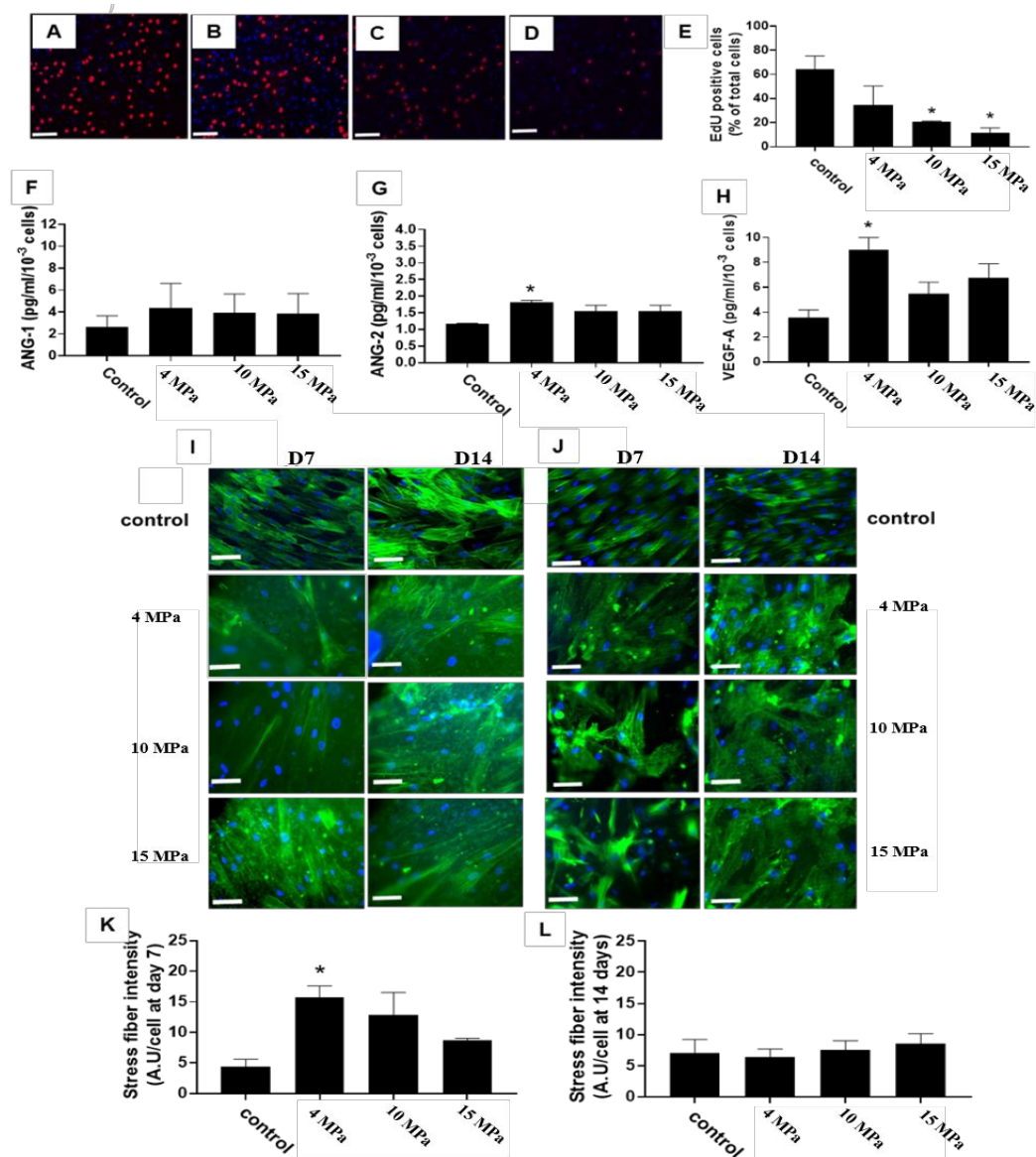
24

F**igure 8. Effect of stiffness on CP proliferation and angiocrine activity: (A)** Fluorescent microscopic image of proliferating control CPs on plastic, (**B**) 2X , (**C**) 5X and (**D**) 8X Glu/EDC/NHS scaffolds. Scale bar: 50μm. The red colour represents the nuclei of proliferating cells, and blue represents the DAPI stained nuclei. (**E**) Bar graph showing the quantification of proliferating CPs. Values are mean and SE, N=3 cell lines at passage 5 of culture. ANOVA, P<0.05; Tukey's multiple comparisons test adjusted P values. *P<0.05 vs control. (**F-H**) Bar graphs show the amount of ANG-1 (**F**), ANG-2 (**G**) and VEGF-A (**H**) secreted by CPs when cultured on scaffolds or plastic (control). Values are mean and SE, N=3 cell lines at passage 5 of culture. ANOVA, P<0.05; Tukey's multiple comparisons test adjusted P values. *P<0.05 vs control. (**I&J**) Immunofluorescence microscopy images show the positive expression of CPs for α-SMA (**I**) and calponin (**J**) following exposure to inductive media. Green colour represents F-actin stained cytoskeleton, and blue colour is DAPI stained nuclei. Scale bar: 50μm. (**K&L**) Bar graphs showing the mean stress fiber intensity in controls (CPs on glass), or 2X (4 MPa), 5X (10 MPa) and 8X (15 MPa) Glu/EDC/NHS scaffolds after seven (**K**) and fourteen days (**L**) from exposure to the differentiation media. Values are mean and SE, N=3 cell lines at passage 5 of culture. ANOVA, P<0.05; Tukey's multiple comparisons test adjusted P values. *P<0.05 vs control.

25

4. Discussion

This study suggests that CPs from the hearts of patients with CHD are influenced by the changes in the matrix stiffness, acquiring a proliferative and angiocrine phenotype and modifying the shape of the cytoskeleton stress fibers when incorporated into softer 3D matrices with larger fiber diameter.

Currently, a great deal of research is focusing on various types of fibers and how they interact with progenitor cells to drive differentiation into specific cell lineages.[30-32] An ideal ECM substrate should be biocompatible, highly porous, biodegradable and mechanically durable depending upon the application.[33] Nanofibrous scaffolds can be fabricated with tunable porosity and mechanical properties, and their 3D architecture can enhance cell adhesion, alter focal-adhesion signalling cascades, and thereby the cell fate.[34, 35] Similarly, the high surface to volume ratio of nanofibrous scaffolds can aid better cell adhesion, proliferation and differentiation.[36] Nanofibrous mimics of the natural ECM could help a better understanding of cell behaviour in their native environment. Moreover, manipulating the physical properties of these mimics provides unique opportunities for regenerative medicine.

One main milestone in our study was the fabrication of a scaffold made of electrospinning gelatin nanofibers in aqueous solution. Previous studies showed that it is impossible to spin gelatin in a pure water solvent because of its polyelectrolytic nature and strong hydrogen bonds reducing the mobility of polymer chains.[37] Hence, high-polarity solvents are required to break the links between the polymer chains and to change the helical structure to random-coil. However, organic solvents have the disadvantage of not being biocompatible.[22] Therefore, we opted for electrospinning gelatin in a pure water solvent, approaching this challenge by raising the environmental temperature (40°C) and humidity (above 50%) using a hot plate and ultrasound nebuliser and by keeping the whole setup in an

26

enclosed incubator. We also used a double-barrel syringe to introduce cross-linking agents during electrospinning to make uniformly cross-linked gelatin nanofibers with defined morphology and mechanical properties. Since the cross-linking reaction between gelatin and EDC/NHS occurred as soon as they were mixed,[38] the processing window needed to be carefully controlled in order not to compromise the electrospinnability, as the viscosity of the solution increased with the increasing crosslink degree. The 10:1 double-barrel syringe was chosen to serve this purpose. Moreover, to aid electrospinning, the voltage was augmented with a reduced flow rate accordingly.

The morphological characterisation of gelatin nanofibrous scaffolds revealed a considerable reduction in the fiber dimensions owing to the progressive increase in cross-linking density. This is also due to the synergistic influence of electrospinning parameters, in particular, the increase in applied voltage and the decrease in flow rate being determinants in creating nanofibers with reduced fiber diameter. Moreover, high cross-linking densities can contribute to the shrinkage of the gelatin nanofibers as new bonds are formed between the polymer chains, which in turn can diminish the intermolecular space.

The prepared gelatin nanofibrous scaffolds were well-crosslinked as demonstrated from the Ninhydrin assay and assessment of peak intensities, which indicated a reduction in the amine groups through the interaction with the aldehyde group of Glu and carboxylic group of EDC/NHS. Retention of structural stability by crosslinking with Glu was an essential requisite for subsequent biofunctional studies on living cells. The scaffolds showed higher YM values in the dry state when compared to the scaffolds in the wet state. This could be attributed to the increased rigidity of proteins [29] and the brittle properties attained by the scaffolds in the absence of water.[22] Usually, the YM of nanofibrous scaffolds is in the range of KPa in wet conditions.[39] In our study, the YM of gelatin nanofibers was in the range of MPa, due to the cross-linking nature of EDC/NHS and Glu, which negatively impact on the water absorption capacity of the

scaffolds. Fibers absorb less water as new bonds are formed, and the polymer chains become closer upon cross-linking, which in turn makes the scaffolds to possess higher retraction forces.[40, 41]

The *in vitro* cell studies showed that even subtle changes in the morphological and mechanical properties of the matrix substrate could remarkably influence the behaviour of human cardiac cells. We focused on CPs because of the increasing evidence that these cells modulate cardiovascular repair and remodelling through the interaction with adjacent cells and the surrounding ECM. Birbair et al. reported the presence of two pericyte subtypes in mice, type-1 (Nestin-GFP-/NG2-DsRed+) and type-2 (Nestin-GFP+/NG2-DsRed+), surrounding blood vessels in the heart, lungs, kidneys, spinal cord, and brain.[42] Type-1, but not type-2, pericytes increase and accumulate near the fibrotic tissue in all organs analysed.[42] However, it remains unclear whether cardiac microvascular pericytes could lead to cardiac fibrosis following an ischaemic injury.[43] We have previously identified a clonogenic population of CPs in the heart of patients with CHD and demonstrated that, after exposure to differentiation media, they acquired markers of VSMCs, but failed to differentiate into endothelial cells or cardiomyocytes.[15] In a Matrigel assay, CPs form networks and enhance the network capacity of endothelial cells.[15] Moreover, they produce collagen-1 and release chemo-attractants that stimulate the migration of c-Kit[+] cardiac stromal cells.[15] When seeded onto clinically approved xenograft scaffolds and cultured in a bioreactor, CPs showed the ability to penetrate into and colonize the graft.[15] Extending these findings, here we show that CPs are capable of colonizing and remaining viable within gelatin nanofiber scaffolds. They also exhibited enhanced cell density, proliferation and extensive spreading in the softer substrates while maintaining their antigenic phenotype and stemness features. The elasticity of the scaffolds with higher fiber diameter would have resulted in more focal adhesion points and hence favoured cell retention. The biomimetic nanofibrous structure, which resembles the native ECM, together with the

porous structure favouring essential nutrients and gaseous exchange[44] and the gelatin's ability to support cell adhesion and promote proteolytic degradation,[44] might also have helped CPs to remain viable and proliferate extensively on softer scaffolds.

Cell proliferation capacity has been previously found to increase in response to microenvironment stiffening for other non-cardiac progenitor cell populations.[45, 46] A study on ovine cardiac stromal cells showed high substrate stiffness increased cell proliferation.[14] However, the elastic moduli examined in that study ranged from 18 to 145 kPa, while the range studied here was 263 to 1000 kPA in the wet state. We observed that proliferation decreased with an increase in stiffness. Altogether, this suggests that the proliferation of cardiac stromal cells reaches its peak between 140 and 260 KPa. The reported elastic moduli of myocardium range from normal values of 18 to 60 kPa to 55 to 295 kPa in failing fibrotic hearts. It is tempting to speculate that fibrotic remodelling of the heart might favour the expansion of the stromal cell compartment. More studies are warranted to confirm this possibility.

We previously reported that the proangiogenic capacity of human CP is associated with the release of a number of angiocrine factors.[15] In this study, we found that the release of ANG-2 and VEGF-A was increased when CPs were seeded in softer scaffolds with higher fiber diameter, while ANG-1 was not altered. The ANG/Tie-2 pathway and VEGF-A play vital roles in the paracrine cross-talk between the pericytes and endothelial cells. The Tie-2 receptor is expressed by endothelial cells and can be activated by ANG-1 produced by pericytes, resulting in the induction of survival, proliferation, migration, and anti-inflammatory signals. ANG-2 acts as a partial agonist of Tie-2, inhibiting Tie-2 signalling in the presence of ANG-1, but activating Tie-2 in the absence of ANG-1. Additional experiments allowing larger changes in stiffness are warranted to determine whether the angiogenic activity of CP can be modulated by manipulating the elastic moduli of the matrix.

29

Changes in stiffness did not alter the differentiation capacity of CPs. However, we observed a substantial accumulation and alignment of F-actin fibers in CPs on softer substrates with increased fiber diameter. This is in line with the theory that cells adapt their cytoskeletal organisation to the elastic modulus of the surrounding microenvironment.[47, 48] Cytoskeletal contraction transfers traction forces back to the ECM. In our study, the higher elasticity and fiber diameter of softer scaffolds might have provided enough focal adhesion points that aid the creation and alignment of F-actin stress fibers resulting in the actin polymerisation. Few studies have also reported the enhanced stress fiber formation for scaffolds with higher matrix stiffness.[49-51] The stiffness measured in all these articles are lower than the stiffness tested in this work. Hence from the results we can infer that the relation between stiffness and stress fiber formation is not always directly proportional, but it entirely depends on the magnitude of stiffness and the cells.

5.Conclusions

In summary, we have successfully produced biomimetic gelatin nanofibrous scaffolds in a water solvent system with different matrix stiffness using an *in situ*-cross-linking electrospinning method. The matrices were well cross-linked and maintained excellent structural stability. They also possessed good mechanical properties and were biocompatible for CPs. Gelatin nanofibrous scaffolds that combine low stiffness (≤0.3 MPa in wet condition) and larger fiber diameter (~400 nm) induced better CP adhesion, extensive cell spreading, proliferation and stress fiber formation. These data support the feasibility of modulating the behaviour of human cardiac stromal cells through the manipulation of physical characteristics of the substrate (i.e. fibre diameter and mechanical stiffness). The study has, however, some limitations. We explored a narrow range of matrix stiffness and also limited our observation to a relatively short-duration culture. Further studies are warranted to determine if cellular

changes induced by our scaffolds could be exploited to generate high-performance grafts for surgical correction of cardiac defects.

Supporting Information

Fiber diameter distribution, positive controls for live-dead assay, expression of CPs on scaffolds without inductive media.

Acknowledgements

31

1
2
3
4
5
6
7
8
9
10
11
12
13
14
15
16
17
18
19
20
21
22
23
24
25
26
27
28
29
30
31
32
33
34
35
36
37
38
39
40
41
42
43
44
45
46
47
48
49
50
51
52
53
54
55
56
57
58
59
60

References

1.   Frantz, C.; Stewart, K. M; Weaver, V.M. The extracellular matrix at a glance. *J Cell Sci*. **2010,** 123 (24), 4195-200, DOI: 10.1242/jcs.023820.

2.   Kim, S. H; Turnbull, J; Guimond, S. Extracellular matrix and cell signalling: the dynamic cooperation of integrin, proteoglycan and growth factor receptor. *J Endocrinol*. **2011**, 209 (2), 139-51, DOI: 10.1530/JOE-10-0377.

3.   Bosman, F.T; Stamenkovic, I. Functional structure and composition of the extracellular matrix, *J Pathol*. **2003**, 200 (4), 423-8, DOI: 10.1002/path.1437.

4.   Tsimbouri, P; Gadegaard, N; Burgess, K; White, K; Reynolds, P; Herzyk, P; Oreffo, R; Dalby, M.J. Nanotopographical effects on mesenchymal stem cell morphology and phenotype. *J Cell Biochem*. **2014,** 115 (2), 380-90, DOI: 10.1002/jcb.24673.

5.   Sun, Y; Chen, C.S; Fu, J. Forcing stem cells to behave: A biophysical perspective of the cellular microenvironment. *Annu. Rev. Biophys*. **2012**, 41, 23.1-23.24. DOI:10.1146/042910-155306.

6.   Nava, M. M; Raimondi, M. T; Pietrabissa, R. Controlling self- renewal and differentiation of stem cells via mechanical cues. *J Biomed Biotechnol*. **2012,** 2012,797410.

7.   Nam, J; Johnson, J; Lannutti, J. J; Agarwal, S. Modulation of embryonic mesenchymal progenitor cell differentiation via control over pure mechanical modulus in electrospun nanofibers. *Acta Biomater*. **2011**, 7(4), 1516-1524, DOI: 10.1016/j.actbio.2010.11.022.

8.   Liu, L; Yuan, Q; Shi, J; Li, X; Jung, D; Wang, L; Yamauchi, K; Nakatsuji, N; Kamei, K; Chen, Y. Chemically-defined scaffolds created with electrospun synthetic nanofibers to maintain mouse embryonic stem cell culture under feeder-free conditions. *Biotechnol Lett* **2012,** 34 (10), 1951-7, DOI: 10.1007/s10529-012-0973-9.

9.   Gauthaman, K; Venugopal, J. R; Yee, F.C; Peh, G. S. L; Ramakrishna, S; Bongso, A. Nanofibrous substrates support colony formation and maintain stemness of human embryonic stem cells. *J. Cell. Mol. Med.* **2009**, 13 (9b), 3475-3484, DOI:10.1111/j.1582-4934.2009.00699.x.

10.   Trappmann, B; Chen, C, S. How cells sense extracellular matrix stiffness: a material's perspective. *Curr Opin Biotechnology* **2013**, 24 (5), 948-53, DOI: 10.1016/j.copbio.2013.03.020.

11.   Lv, H; Li, L; Sun, M; Zhang, Y; Chen, L; Rong, Y; Li, Y. Mechanism of regulation of stem cell differentiation by matrix stiffness. *Stem Cell Res Ther*. **2015,** 6 (1), 103, DOI:10.1186/s13287-015-0083-4.

12.   Kohn, J.C; Zhou, D.W; Bordeleau, F; Zhou, A.L; Mason, B.N; Mitchell, M.J; King, M.R; Reinhart-King, C.A. Cooperative effects of matrix stiffness and fluid shear stress on endothelial cell behavior. *Biophys J*. **2015**, 108 (3), 471-8, DOI: 10.1016/j.bpj.2014.12.023

13.   Stout, K.K; Broberg, C.S; Book, W.M; Cecchin, F; Chen, J.M; Dimopoulos, K; Everott, M.D; Gatzoulis, M; Harris, L; Hsu, D.T; Kuvin, J.T; Law, Y; Martin, C.M; Murphy, A.M; Ross, H.J; Singh, G; Spray, T.L. Chronic heart failure in congenital heart disease: A scientific statement from the American Heart Association. *Circulation*. **2016**, 133 (8), 770-801, DOI:10.1161/CIR.0000000000000352.

14.   Qiu, Y; Bayomy, A.F; Gomez, M.V; Bauer, M; Du, P; Yang, Y; Zang, X; Liao, R. A role for matrix stiffness in the regulation of cardiac side population cell function. *Am J Physiol Heart Circ Physiol*. **2015**, 308 (9), H990-7. DOI: 10.1152/ajpheart.00935.2014.

15.   Avolio, E; Rodriguez-Arabaolaza, I; Spencer, H. L; Riu, F; Mangialardi, G; Slater, S. C; Rowlinson, J; Alvino, V. V; Idowu, O. O, Soyombo, S; Oikawa, A; Swim, M. M; Kong, C. H; Cheng, H; Jia, H; Ghorbel, M. T; Hancox, J. C; Orchard, C. H; Angelini, G; Emanueli, C; Caputo, M; Madeddu, P. Expansion and characterization of neonatal cardiac pericytes provides a novel cellular option for tissue engineering in congenital heart disease. *J Am Heart Assoc*. **2015**, 4 (6), e002043, DOI: 10.1161/JAHA.115.002043.

16.   Avolio, E; Meloni, M; Spencer, H. L; Riu, F; Katare, R; Mangialardi, G; Oikawa, A; Rodriguez-Arabaolaza , I; Dang, Z; Mitchell, K; Reni, C; Alvino, V. V; Rowlinson, J; Livi, U; Cesselli, D; Angelini, G; Emanueli, C; Beltrami, A. P; Madeddu, P. Combined intramyocardial delivery of human pericytes and cardiac stem cells additively improves the healing of mouse infarcted hearts through stimulation of vascular and muscular repair. *Circ Res*. **2015,** 116 (10) 81-94, DOI: 10.1161/CIRCRESAHA.115.306146.

17.   Gubernator, M; Slater, S. C; Spencer, H. L; Spiteri, I; Sottoriva, A; Riu, F; Rowlinson, J; Avolio, E; Katare, R; Mangialardi, G; Oikawa, A; Reni, C; Campagnolo, P; Spinetti, G; Touloumis, A; Tavaré, S; Prandi, F; Pesce, M; Hofner, M; Klemens; Emanueli, C; Angelini, G; Madeddu, P. Epigenetic profile of human adventitial progenitor cells correlates with therapeutic outcomes in a mouse model of limb ischemia. *Arterioscler Thromb Vasc Biol*. **2015**, 35 (3), 675-88, DOI:10.1161/ATVBAHA.114.304989.

18.   Katare, R; Riu, F; Mitchell, K; Gubernator, M; Campagnolo, P; Cui, Y; Fortunato, O; Avolio, E; Cesselli, D; Beltrami, A. P; Angelini, G; Emanueli, C; Madeddu, P. Transplantation of human pericyte progenitor cells improves the repair of infarcted heart through activation of an angiogenic program involving micro-RNA-132. *Circ Res*. **2011**, 30, 109 (8), 894-906, DOI: 10.1161/CIRCRESAHA.111.251546.

19.   Campagnolo, P; Cesselli, D; Al Haj Zen, A; Beltrami, A.P; Krankel, N; Katare, R; Angelini, G; Emanueli C; Madeddu P. Human adult vena saphena contains perivascular progenitor cells endowed with clonogenic and proangiogenic potential. *Circulation*. **2010,** 121 (15), 1735-45, DOI:10.1161/CIRCULATIONAHA.109.899252.

20.   Bernstein, H. S; Srivastava, D. Stem cell therapy for cardiac disease. *Pediatr Res*. **2012**, 71(4), 491-9, DOI:10.1038/pr.2011.61.

21.   Fuoco, C; Sangalli, E; Vono, R; Testa, S; Sacchetti, B; Latronico, M. V; Bernardini, S; Madeddu, P; Cesareni, G; Seliktar, D; Rizzi, R; Bearzi, C; Cannata, S. M; Spinetti, G; Gargioli, C. 3D hydrogel environment rejuvenates aged pericytes for skeletal muscle tissue engineering. *Front Physiol*. **2014**, 30 (5), 203, DOI:10.3389/fphys.2014.00203.

22.   Zhang, Y.Z; Ouyang, H.W; Lim, C.T; Ramakrishna, S; Huang, Z.M. Electrospinning of gelatin fibers and gelatin/PCL composite fibrous scaffolds. *J Biomed Mater Res Part B Appl Biomater*. **2005**;72(1):156-65, DOI:10.1002/jbm.b.30128.

23. Zhang, S; Huang, Y; Yang, X; Mei, F; Ma, Q; Chen, G; Ryu, S; Deng, X. Gelatin nanofibrous membrane fabricated by electrospinning of aqueous gelatin solution for guided tissue regeneration. *J Biomed Mater Res*. **2008**, 3, (90A), 671-679, DOI: 10.1002/jbm.a.32136.

24.   Zhang, Y.Z; Venugopal, J; Huang, Z. M; Lim, C. T; Ramakrishna, S.. *Polymer,* **2006,** 47 (8) 2911–2917, DOI:10.1016/j.polymer.2006.02.046.

25.   Lai, J. Y; Li, Y. T; Cho, C. H; Yu, T.C. Nanoscale modification of porous gelatin scaffolds with chondroitin sulphate for corneal stromal tissue engineering. *Int J Nanomedicine* **2012,** 7, 1101–1114, DOI:10.2147/IJN.S28753.

26.   Carrabba, M; Maria, C. D; Oikawa, A; Reni, C; Rodriguez-Arabaolaza, I; Spencer, H; Slater, S; Avolio, E; Dang, Z; Spinetti, G. Design, fabrication and perivascular implantation of bioactive scaffolds engineered with human adventitial progenitor cells for stimulation of arteriogenesis in peripheral ischemia. *Biofabrication.* **2016,** 8 (1), 1758-5090, DOI:10.1088/1758-5090/8/1/015020.

27.   Xu, J. G; Zhu, S.Y; Heng, B.C; Dissanayaka, W.L; Zhang, C.F. TGF-β1-induced differentiation of SHED into functional smooth muscle cells. *Stem Cell Res Ther*. **2017** 8 (10), DOI:10.1186/s13287-016-0459-0.

28.   Davidenko, N; Schuster, C.F; Bax, D.V; Raynal, N; Farndale, R.W; Best, S.M; Cameron,R.E. Control of crosslinking for tailoring collagen-based scaffolds stability and mechanics. *Acta Biomater*. **2015**, 25, 131-42, DOI: 10.1016/j.actbio.2015.07.034.

29.   Dias, J.R; Baptista-Silva, de Oliveira, S.C.M.T; Sousa, A; Oliveira, A.L; Bártolo, P.J; Granja, P.L. *Eur. Polym. J.* **2017**, (95), 161-173, DOI:10.1016/j.eurpolymj.2017.08.015.

30.   Mahairaki, V; Lim, S. H; Christopherson, G. T; Xu, L; Nasonkin, I., Yu, C; Mao, H.Q; Koliatsos, V.E. Nanofiber matrices promote the neuronal differentiation of human embryonic stemcell-derived neural precursors in vitro. *Tissue Eng Part A* **2011**, 17 (5-6), 855- 63, DOI: 10.1089/ten.TEA.2010.0377.

31.   Li, W. J; Tuli, R; Okafor, C; Derfoul, A; Danielson, K. G; Hall, D. J; Tuan, R.S. A three-dimensional nanofibrous scaffold for cartilage tissue engineering using human mesenchymal stem cells. *Biomaterials* **2005**, 26 (6), 599-609, DOI:10.1016/j.biomaterials.2004.03.005.

32.   Kang, X; Xie, Y; Powell, H. M; James Lee, L; Belury, M. A; Lannutti, J. J; Kniss, D.A. Adipogenesis of murine embryonic stem cells in a three-dimensional culture system using electrospun polymer scaffolds. *Biomaterials* **2007**, 28 (3), 450-458 DOI:10.1016/j.biomaterials.2006.08.052.

33.   Kumar, P.T.S; Praveen, G; Raj, M; Chennazhi, K. P; Jayakumar, R.. *RSC Adv.* **2014**, 4(110), 65081-7, DOI:10.1039/C4RA11969J.

34.   Nur-E-Kamal, A; Ahmed, I; Kamal, J; Schindler, M; Meiners, S. Three-dimensional nanofibrillar surfaces promote self-renewal in mouse embryonic stem cells. *Stem Cells* **2006,** 24 (2), 426-433, DOI:10.1634/stemcells.2005-0170.

35.   Xia, H; Nho, R. S; Kahm, J; Kleidon, J; Henke, C. A. Focal adhesion kinase is upstream of phosphatidylinositol 3-kinase/Akt in regulating fibroblast survival in response to contraction of type I collagen matrices via a beta one integrin viability signalling pathway. *J Biol Chem* **2004**, 279 (31), 33024-34, DOI:10.1074/jbc.M313265200.

36.   Wu, S; Chang, W; Dong, G; Chen, K; Chen, Y; Yao, C. Cell adhesion and proliferation enhancement by gelatin nanofiber scaffolds. *J Bioact Compat Pol.* **2011,** 26 (6), 565-577, DOI:10.1177/0883911511423563.

37.   Huanga, Z-M; Zhang, Y.Z; Ramakrishna, S; Limb, C.T. Electrospinning and mechanical characterization of gelatin nanofibers. *Polymer* **2004,** 45, 5361–5368. DOI: 10.1016/j.polymer.2004.04.005.

38.   Kuijpers, A.J; Engbers, G.H.M; Feijen, J; De Smedt, S.C; Meyvis, T.K.L; Demeester, J; Krijgsveld J; Zaat, S.A.J; Dankert, J. Characterization of the network structure of carbodiimide cross-linked gelatin gels. *Macromolecules*. **1999**, 32 (10), 3325-33. DOI:10.1021/ma981929v.

39.   Jiang, X; Nai, M.H; Lim, C.T; Le Visage, C; Chan, J.K.Y; Chew, S.Y. Polysaccharide nanofibers with variable compliance for directing cell fate. *J of Biomed Mater Res Part A.* **2014**,103(3),959-68, DOI:10.1002/jbm.a.35237.

40.   Martucci, J.F; Espinosa, J.P; Ruseckaite, R.A. Physicochemical Properties of Films Based on Bovine Gelatin Cross-linked with 1,4-Butanediol Diglycidyl Ether. *Food Bioprocess Tech.* **2015**;8(8):1645-56, DOI:10.1007/s11947-015-1524-x.

41.   Vargas, G; Acevedo, J.L; Lopez, J; Romero, J. Study of cross-linking of gelatin by ethylene glycol diglycidyl ether. *Mater. Lett.* **2008**, 62 (21-22), 3656-8, DOI: 10.1016/j.matlet.2008.04.020.

42.   Birbrair, A; Zhang, T; Files, D.C; Mannava, S; Smith, T; Wang, Z.M; Messi, M.L; Mintz, A; Delbono, O. Type-1 pericytes accumulate after tissue injury and produce collagen in an organ-dependent manner. *Stem Cell Res Ther*. **2014**, 5 (6), 122, DOI: 10.1186/scrt512.

43.   Siao, C.J; Lorentz, C.U; Kermani, P; Marinic, T; Carter, J; McGrath, K; Padow, V.A; Mark, W; Falcone, D.J; Cohen-Gould, L; Parrish, D.C; Habecker, B.A; Nykjaer, A; Ellenson, L.H; Tessarollo, L; Hempstead B.L. ProNGF, a cytokine induced after myocardial infarction in humans, targets pericytes to promote microvascular damage and activation. *J Exp Med.* **2012**, 209 (12), 2291-305. DOI: 10.1084/jem.20111749.

44.   Liu, Y.X; Chan-Park, M.B. A biomimetic hydrogel based on methacrylated dextran-graft-lysine and gelatin for 3D smooth muscle cell culture. *Biomaterials*. **2010**, 31(6),1158-70, DOI:10.1016/j.biomaterials.2009.10.040.

45.   Evans, N.D; Minelli, C; Gentleman, E; LaPointe, V; Patankar, S,N; Kallivretaki, M; Chen, X; Roberts, C.J; Stevens, M.M. Substrate stiffness affects early differentiation events in embryonic stem cells. *Eur Cell Mater*. **2009**, 18, 1-13, DOI:10.22203/eCM.

46.   Rowlands, A.S; George, P.A; Cooper-White, J.J. Directing osteogenic and myogenic differentiation of MSCs: interplay of stiffness and adhesive ligand presentation. *Am J Physiol Cell Physiol.* **2008**, 295 (4), C1037-44, DOI: 10.1152/ajpcell.67.2008.

47.   Ingber, D.E. Tensegrity 1:Cell structure and hierarchical systems biology. *J Cell Sci* **2003**, 116, 1157–73, DOI:10.1242/jcs.00359.

48.   Wozniak, M. A; Chen, C. S. Mechanotransduction in development: A growing role for contractility. *Nat Rev Mol Cell Biol*. **2009**, 10 (1), 34–43, DOI:10.1038/nrm2592.

49.   Sun, Y; Deng, R; Ren, X; Zang, K; Li, J. 2D Gelatin methacrylate hydrogels with tunable stiffness for investigating cell behaviours. *ACS Appl. Bio Mater.* **2019,** 1 (2), 570-576, DOI: 10.1021/acsabm.8b00712.

50.   Sun, Y; Zang, K; Deng, R; Ren, X; Wu, C; Li, J. Tunable stiffness of graphene oxide/polyacrylamide composite scaffolds regulates cytoskeleton assembly. *Chem. Sci*. **2018**,31 (9), 6516-6522, DOI:10.1039/C8SC02100G.

51.   Zhang, K; Gao, H; Deng, R; Li, J. Emerging applications of nanotechnology for controlling cell-surface receptor clustering. *Angew. Chem. Inter. Ed*. **2019**, 15 (58), 4790-4799 DOI: 10.1002/anie.201809006.

1
2
3
4
5
6
7
8
9
10
11
12
13
14
15
16
17
18
19
20
21
22
23
24
25
26
27
28
29
30
31
32
33
34
35
36
37
38
39
40
41
42
43
44
45
46
47
48
49
50
51
52
53
54
55
56
57
58
59
60

Abstract/TOC Graphic